Icarus 230 (2014) 143–150

Contents lists available at ScienceDirect

Icarus

journal homepage: www.elsevier.com/locate/icarus

Basaltic sand ripples at Eagle Crater as indirect evidence for the hysteresis effect in martian saltation

H. Yizhaq [a,*], J.F. Kok [b], I. Katra [c]

[a] Solar Energy and Environmental Physics, BIDR, Ben-Gurion University of the Negev, Midreshet Ben-Gurion, Israel
[b] Department of Atmospheric and Oceanic Sciences, University of California, Los Angeles, California, USA
[c] Department of Geography and Environmental Development, Ben-Gurion University of the Negev, Beer Sheva 84105, Israel

ARTICLE INFO

Article history:
Available online 14 August 2013

Keywords:
Mars
Aeolian processes
Mars surface

ABSTRACT

The rover Opportunity documented small basaltic sand ripples at the bottom of Eagle Crater, Meridiani Planum on Mars. These ripples are composed of fine basaltic sand (~100 μm diameter) and their average wavelength and height are 10 cm and 1 cm, respectively. Present theories on the transition between saltation and suspension predict that such light particles are suspended by turbulence at the fluid threshold, which is the minimum wind speed required to initiate saltation. Consequently, the existence of these ~100 μm ripples on Mars indicates that either current suspension theories are incorrect, or that saltation can take place at wind speeds substantially below the fluid threshold. Indeed, recent studies point to the occurrence of hysteresis in martian saltation. That is, once initiated, hysteresis can be maintained at much lower wind speeds than the fluid threshold. We investigated the possible role of hysteresis in the formation of fine-grained ripples on Mars by coupling, for the first time, a detailed numerical saltation model (COMSALT) with a dynamic model for sand ripple formation. The results from the coupled model indicate that ripples with properties similar to those observed at Eagle Crater can be developed by the impact mechanism at shear velocities far below the fluid threshold. These findings are consistent with the occurrence of hysteresis in martian saltation, and support the hypothesis that hysteresis plays a role in the surprisingly large sand mobility observed at several locations on Mars.

1. Introduction

The martian surface displays an abundance of aeolian bedforms such as ripples, megaripples, and different types of dunes (Bourke et al., 2010; Kok et al., 2012). Because of Mars' thin atmosphere, it was thought that very strong winds are required for sand transport (Iversen and White, 1982) and some studies thus proposed that most aeolian bedforms are relict forms from a past, windier climate (Merrison et al., 2007; Bourke et al., 2008; Zimbelman et al., 2009). However, recent studies have provided increasing evidence that many aeolian features on Mars are active (Jerolmack et al., 2006; Sullivan et al., 2008; Silvestro et al., 2010; Chojnacki et al., 2011; Bridges et al., 2012a,b), and that aeolian activity is much more abundant on Mars than previously thought. For instance, the Nili Patera dune field experiences sand fluxes that are of the same order of those in the Victoria Valley on Earth (Bridges et al., 2012b). This substantial aeolian activity occurs despite atmospheric circulation models predicting that large-scale winds generally remain well below the fluid threshold necessary to initiate sand transport (Haberle et al., 1993; Basu et al., 2004), even in areas where active transport is observed (Chojnacki et al., 2011). However, small-scale winds triggered by convection or small-scale topography can substantially exceed the large-scale winds, and could occasionally initiate saltation (Fenton and Michaels, 2010). Sporadic and limited wind measurements made by Mars landers have also found that winds on Mars rarely exceed the sand transport fluid threshold (Schofield et al., 1997; Zimbelman, 2000; Holstein-Rathlou et al., 2010).

One of the possible explanations for resolving the discrepancy between observations of aeolian activity and the apparent scarcity of winds strong enough to initiate saltation is that most sand transport on Mars occurs below the fluid threshold (Kok, 2012). This is possible because, once saltation has been initiated on Mars, it can likely be sustained by wind speeds that are only a fraction of the fluid threshold (Claudin and Andreotti, 2006; Kok, 2010a,b). The threshold wind speed that is required to sustain saltation after initiation is termed the impact threshold. On Earth, the wind speed required to sustain saltation after initiation, termed the impact threshold, is ~80% of the fluid threshold (Bagnold, 1941). But on Mars, the impact threshold is expected to be only ~10% of the fluid threshold (Kok et al., 2012). This occurs because the lower martian gravity and air density allow sand grains to travel in higher and

* Corresponding author.
E-mail addresses: yiyeh@exchange.bgu.ac.il (H. Yizhaq), jasperkok@cornell.edu (J.F. Kok), katra@bgu.ac.il (I. Katra).

0019-1035/$ - see front matter © 2013 Elsevier Inc. All rights reserved.
http://dx.doi.org/10.1016/j.icarus.2013.08.006

longer trajectories on Mars at a given launch speed, causing them to be accelerated by wind for a longer duration in a single hop than on Earth (Edgett and Christensen, 1991, 1994; Edgett, 2002). Thus, upon impact, these grains have gathered more speed than they would have on Earth, allowing saltation to propagate itself by the ejection (*splashing*) of surface particles by impacting saltating particles at much lower wind speeds than the fluid threshold required to initiate it (Kok, 2010a). However, this proposed occurrence of *hysteresis* in martian saltation is based on numerical and analytical models (Claudin and Andreotti, 2006; Almeida et al., 2008;Kok, 2010a,b; Pähtz et al., 2012), and not on in situ observations or wind tunnel experiments. Here, we provide an experimental test of the occurrence of hysteresis in martian saltation by comparing the predictions of a numerical ripple model for wind shear velocities below the fluid threshold with the observations of ripples by the Mars Exploration Rovers (Sullivan et al., 2005; Squyres et al., 2006).

Meridiani Planum is one of the most extensively studied regions on Mars (Chojnacki et al., 2011). At the Opportunity landing site, ripples (of mixed particle sizes) and occasional wind streaks (dark and light) are quite common (Sullivan et al., 2005). Among the bedforms observed at Eagle Crater in Meridiani Planum are ripples composed almost entirely of basaltic 100 μm sand grains (measured by the Microscopic Imager, Sullivan et al., 2005; see Fig. 1). These ripples are found within craters, smaller pits, and structural troughs that apparently serve as particle traps and were observed by the Mars Exploration Rover Opportunity (Fig. 2g in Sullivan et al. (2005) and Squyres et al. (2006)) at Meridiani Planum.

These sand ripples were examined on the floor of Eagle Crater and on drifts among the outcrops of Eagle Crater. Their mean height is 1 cm and their longest wavelength is 11 cm. The Eagle floor ripples occur in several distinct patches with different characteristic wavelengths. These bedforms are probably currently mobilized by the same recent winds that formed the bright wind streaks associated with Eagle Crater and other craters in the area (Sullivan et al., 2005; Squyres et al., 2006).

The apparent saltation of 100 μm particles on Mars, deduced from the existence of basaltic ripples, was a surprise compared to previous predictions that saltation particle sizes on Mars are several times larger (Edgett and Christensen, 1991; Sullivan et al., 2005; Parteli and Herrmann, 2007). In particular, these 100 μm particles are thought to become suspended by winds below the fluid threshold, which would make them unable to form bedforms. Note that the exact wind speed at which particles become suspended is difficult to quantify because the occurrence of suspension depends on the turbulent wind field, making suspension a highly stochastic process (e.g., Anderson, 1987a). Nonetheless, current theories predict that, once the wind shear velocity u_* becomes of the order of the particle terminal velocity (v_t), suspension of particles will become important (Greeley and Iversen, 1985; Edgett and Christensen, 1991). For 100 μm particles on Mars, this occurs for $u_* \approx 0.4$ m/s (Kok et al., 2012), and thus well below the fluid threshold, estimated at ~1.5 m/s (Iversen and White, 1982; Greeley and Iversen, 1985). Since this result implies that most particles would be in suspension at the fluid threshold and thus unable to form bedforms, Sullivan and colleagues proposed that the suspension criteria of $u_*/v_t = 1$ is not appropriate for Mars (Sullivan et al., 2005; Sullivan and Banfield, 2005), although other studies have disputed this (Jerolmack et al., 2006).

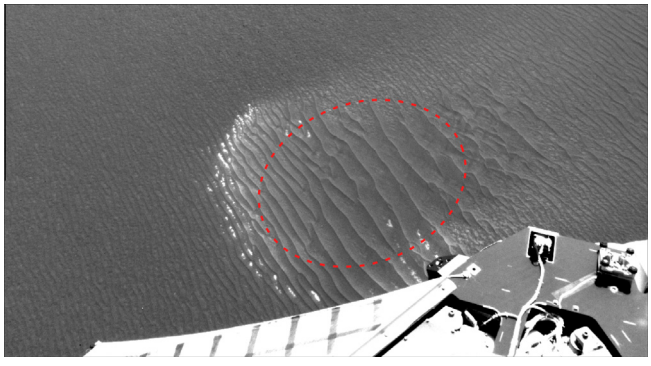

Fig. 1. This Navcam camera view was obtained by the Mars Exploration Rover "Opportunity" on the fifth day of its mission, and shows ripples on the floor of 20 m-wide Eagle Crater. Ripples in the circled area have 3–11 cm spacing, and Microscopic Imager views of this area obtained later showed open pore space among the ~100 μm grains at the surface, indicating the ripples are not relicts but were recently active.

An alternative explanation for the occurrence of 100 μm ripples on Mars is that hysteresis allows saltation, and thus bedform formation, to occur well below the fluid threshold. In particular, a high-speed turbulent eddy could lift several surface particles and possibly suspend them (Greeley and Iversen, 1985; Jerolmack et al., 2006). But since $v_t \approx 0.4$ m/s for 100 μm particles, the lifted particles would exit the high-speed eddy within seconds. If the mean wind is not too strong, the lifted particles would return to the surface and, upon impact, would initiate saltation by splashing surface particles. Because of the low martian impact threshold, saltation could then be sustained downwind for wind speeds substantially below the fluid threshold. Note that if the wind exceeded the fluid threshold for a long period of time, raised particles would remain in suspension, and thus too few would fall to the surface to initiate saltation. However, as described above, we envisage a scenario in which only a small fraction of wind speeds (associated with individual turbulent eddies) are above threshold, which results in some particles being raised but not remaining in suspension for very long before falling back to the surface, enabling saltation to be initiated downwind.

Our main goal here is thus to test whether the 100 μm basaltic ripples at Eagle Crater could be formed under winds which are intermediate between the fluid threshold [estimated at ~1.5 m/s; (Greeley and Iversen, 1985)] and the impact threshold [predicted at ~0.1–0.3 m/s; Kok, 2010a,b; Pähtz et al., 2012]. If so, the existence of these small basaltic ripples can be interpreted as support for the hysteresis effect in martian saltation. To achieve this goal, we used the numerical saltation model COMSALT (Kok and Renno, 2009) to drive a dynamic model for sand ripple formation (Yizhaq et al., 2004), and compared the results against the observations of Sullivan et al. (2005).

The outline of this paper is as follows: We first present the ripple model, then we show the COMSALT calculation results of the parameters used by the ripple model. We then show the results of the ripple model under different shear velocities. We end with conclusions regarding the sand transport mechanism on Mars.

2. Methodology

2.1. The impact ripple model

When the wind exceeds the fluid threshold, saltation is initiated by the aerodynamic lifting of sand grains. When these grains return to the surface, they impart their energy and momentum to the bed and eject other grains into motion. Experimental results (Anderson, 1987b; Beladjine et al., 2007) indicate that this bombardment process generates two populations of moving grains. The first population consists of grains that are ejected with large energy, reach higher elevations and are accelerated by the wind. These grain form the "saltating" population. The second population consists of grains that are ejected ('splashed') with low energy, stay near the surface, and move forward in small hops of several grain diameters. These crawling grains form the 'reptating' population.

The mean number of ejected grains varies nearly linearly with the impact speed of the saltating particles (Rioual et al., 2003).

To simulate the formation of ripples in Meridiani Planum, we use the ripple model of Yizhaq et al. (2004), which is based on the classic approach of Anderson (1987b) and includes a correction to the reptation flux that depends on the local bed slope. According to Anderson's model, the sole role of saltating grains is to bring energy into the system, extracting it from the wind that blows above the surface of the sand. The basic geometry of the problem is shown in Fig. 2. Within this view, ripple formation is entirely due to the spatial variability of the reptation flux. The saltation flux is considered spatially uniform and does not directly contribute to ripple formation due to the low exchange flux between saltating and reptating particles. In this view the saltating grains have uniform trajectories and impact angles as shown in Fig. 2 (mathematically we assume that $\partial Q_s/\partial x = 0$ where Q_s is the saltation flux). Because the saltating grains are spatially uniform, spatial change in the reptation flux is only due to a change in bed topography. In particular, the windward slopes of small bumps on the sand surface are subjected to more impacts than the lee slopes. The flux of reptating flux is therefore higher uphill than downhill, which causes the bumps to increase in size. This instability of the flat bed to small undulations drives ripple formation, and is termed the "screening instability" (Kok et al., 2012). The downwind sides of the bumps act as "shadow zones" where particles are sheltered from the impact of saltating grains, so more sand is accumulated, leading to the growth of the initial perturbations.

We represented the above processes in a one dimensional model of sand transport based on the Exner equation, which expresses the conservation of mass (Yizhaq et al., 2004):

$$(1-\lambda_p)\rho_p \frac{\partial h}{\partial t} = -\frac{\partial Q}{\partial x}, \tag{1}$$

where $h(x,t)$ is the local height of the sand surface at point x and time t, λ_p is the porosity of the bed, ρ_p is the particle density and Q is the reptation flux at a certain point and time obtained by the sum of all the grains that pass that point at that time. As discussed in the next section, the probability distribution of reptation lengths $p(\alpha)$ (defined as $\int_0^\infty p(\alpha)d\alpha = 1$) will be calculated by our numerical steady state saltation model COMSALT (see Section 2.2). Following Anderson (1987b), we derive an explicit expression for reptation flux

$$Q = mn \int_0^\infty d\alpha p(\alpha) \int_{x-\alpha}^{x} N_{im}(x')dx', \tag{2}$$

where m is the mass of each particle, and n is the average number of reptating grains ejected by the impact of one saltating grain (also computed by COMSALT). Because saltation flux is uniform and the fixed angle ϕ, at which the grains descend back to the ground, is assumed to be constant, the number density of impacting grains changes only because of the variations in the bed slope. Based on geometrical considerations (Anderson, 1987b), we obtain

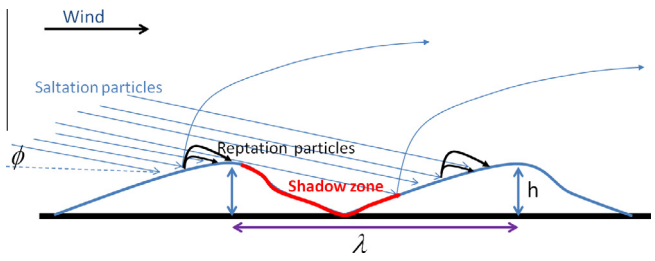

Fig. 2. Schematic view of typical ripples. Saltating grains approach the windward slope at angle ϕ. Upon impact, these particles eject reptating grains, whereas the saltating grains ricochet. h is the ripple height and λ is the wavelength.

$$N_{im}(x) = N_{im}^0 \frac{1 + h_x \cot\phi}{\sqrt{1+h_x^2}}, \tag{3}$$

where $h_x = \partial h/\partial x \equiv \tan\theta$, where θ is the angle the bed makes with the horizontal, and N_{im}^0 is the number density of impacting grains on a flat surface. We further modify Eq. (2) to take into account a correction of the reptation length on an inclined plane (Yizhaq et al., 2004). This correction leads to a mean reptation length that is shorter on the windward slope and longer on the leeward slope of the bedform. The full model can be written as:

$$h_t = -Q_0 \partial_x[(1-\mu)Q], \tag{4}$$

where the subscript t denotes differentiation with respect to time and subscript x denotes differentiation with respect to space. The parameter μ heuristically includes the correction to reptation flux discussed above, and $Q_0 = mnN_{im}^0 \cot\phi/\rho_b(1-\lambda_p)$. The basic parameters used by the ripple model – N_{im}^0, n and $p(\alpha)$ – will be computed by COMSALT under martian conditions. Substituting Eqs. (2) and (3) in Eq. (4) leads to the following equation:

$$h_t = Q_0\left\{\mu h_{xx}\int_0^\infty d\alpha p(\alpha)\int_{x-\alpha}^{x} F(x')dx' + (1-\mu h_x)\int_0^\infty d\alpha p(\alpha)[F(x-\alpha)-F(x)]\right\}, \tag{5}$$

where h_{xx} is the second derivative of h with respect to space and $F(x) = (\tan\phi + h_x)/\sqrt{1+h_x^2}$. Eq. (5) breaks down when the lee slope of the ripple exceeds the impact angle ϕ of the saltating grains. In such conditions, the ratio N_{im}/N_{im}^0, where $N_{im}(x) = N_{im}^0(1 + h_x \cot\phi)$ is the impact density on the inclined slope, becomes unphysically negative (Anderson, 1987b). In these cases we add the restriction $F(x) = 0$. We also applied this condition for the shadow zone where the impact rate is zero (see Fig. 2). Thus, we used a complete shadowing effect (Sharp, 1963; Manukyan and Prigozhin, 2009) below the line defined by the saltation path of a grain which touches the crest (see Fig. 2). The values of the parameters used in the numerical ripple simulations are summarized in Table 1. Note that, although not listed in Table 1, the wind shear velocity u_* indirectly enters the ripple model by using parameter values calculated by COMSALT for different shear velocities.

The ripple model equation (Eq. (5)) was solved numerically by using an explicit second-order finite difference scheme with periodic boundary conditions starting from random initial conditions. The integral terms were computed by using the composite trapezoid rule, and the time integration was carried out by using the second-order Adams–Bashforth rule (Fausett, 1999). The grid was comprised of 2048 points for a spatial dimension of 2 m (i.e., spatial resolution of approximately 1 mm) and a time step of 0.005 s. The wind velocity and wind direction are assumed to be constant during the simulation. Although ripples on Earth can be formed within minutes (Anderson, 1990; Andreotti et al., 2006), the lower martian air density results in a much lower saltator impact rate on Mars ($\sim 10^6$ m^{-2} s^{-1} for $u_* = 0.5$ m/s; Fig. 3b) than on Earth ($\sim 10^8$ for $u_* = 0.5$ m/s), making the ripple formation much slower. Thus, we chose to run the ripple model for a period of 25 Earth hours, which is close to one martian day (sol, which is equal to 24.67 Earth hours).

2.2. The numerical saltation model (COMSALT)

We use COMSALT (Kok and Renno, 2009), a numerical model for steady-state saltation, to calculate the input parameters of our ripple model for martian conditions. COMSALT simulates the trajectories of saltating particles under the influence of gravitational and fluid forces. The effects of turbulence on particle trajectories is treated as described in Kok and Renno (2009), except that we adjusted the treatment of the Lagrangian turbulence coherence

Table 1
Description of the model parameters and their values used in the simulations.

Parameter	Description	Value
ρ	Grain density (basaltic sand)	3000 kg/m^3
m	Grain mass	Calculated for spherical grains with a diameter of 100 μm
λ_p	Bed porosity	0.35
ϕ	Impact angle of saltation particles	10°
μ	Correction to the reptation length on a slope (related to the ejection angle of the reptation particle)	0.839
N_{im}^0	The number of saltating grains impacting a flat surface per unit area and time	Calculated by COMSALT under Mars atmospheric conditions for different shear velocities
n	The average number of ejected grains per impact of a saltating grain	As above
$p(\alpha)$	The probability distribution of reptation lengths	As above

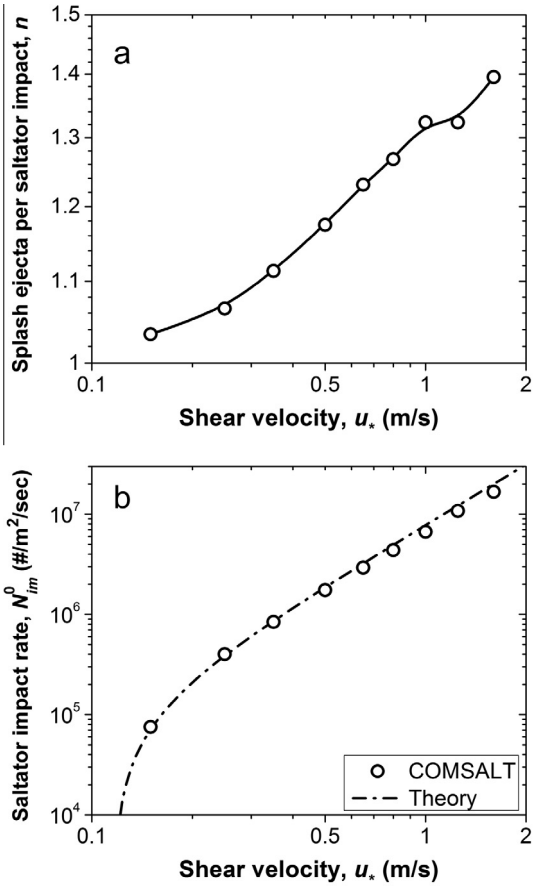

Fig. 3. COMSALT simulations of (a) the number of splashed particles per impacting saltator n, and (b) the number of impacting saltators per unit time and area N_0^{im}, both for saltation of 100 μm basalt particles under martian conditions. Also included for comparison is the theoretically predicted scaling of the flux of impacting saltating grains (dash-dotted line) with $(u_*^2 - u_{*it}^2)$, where u_{*it} is the shear velocity at the impact threshold (Shao et al., 1993; Kok et al., 2012). We have defined a saltator as a particle that rebounds from the surface at least once, and a reptator as a particle that does not rebound after ejection.

timescale (T_L) because the Kok and Renno (2009) treatment proved unstable for small particles on Mars. Specifically, we followed Wilson and Sawford (1996) and Nemoto and Nishimura (2004), and used

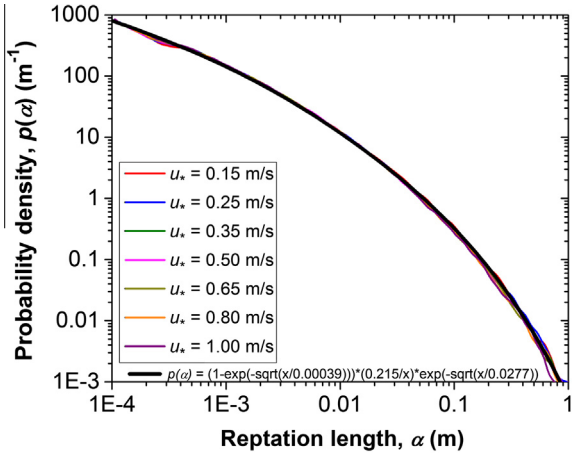

Fig. 4. COMSALT simulations for the probability distribution of reptation lengths for transport of 100 μm particles at different shear velocities.

$$T_L = \frac{0.4z}{u_*}, \tag{6}$$

where z is the height from the surface. Most particles in our numerical simulation do not enter suspension for $u_* < 1$ m/s. This occurs in part because small particles saltate close to the surface (Kok and Renno, 2009), where the turbulence coherence time is small compared to the particles' response time (see Eq. (6)), making suspension unlikely (Sullivan and Banfield, 2005).

COMSALT also simulates the retardation of the wind profile by the drag of saltating particles, which is the process that ultimately limits the number of particles that can be saltating at any given time. Moreover, COMSALT uses a parameterization based on the conservation of energy and momentum to account for the splashing (ejection) of surface particles. This parameterization is in good agreement with a range of laboratory experiments, including measurements of the number and speed of ejected particles. The realistic parameterization of splash is especially important for the current application of calculating the properties of 100 μm reptating particles for use by the ripple model.

Since 100 μm particles on Mars are thought to experience substantial cohesive forces, we accounted for the effect of these forces on the splash process following the treatment of Kok (2010b). As expected, we find that the main effect of cohesive forces is a reduction of the number of reptating particles produced per saltation impact (defined as n in the ripple model).

3. Results and discussion

We ran COMSALT to model saltation of 100 μm basalt particles at martian conditions (air pressure 700 Pa, air temperature 220 K, gravitational acceleration 3.72 m s^{-2}, particle density 3000 kg m^{-3}, and dynamic viscosity 1.1×10^{-5} kg m^{-1} s^{-1}), and simulated the essential parameters required for the ripple evolution model as indicated in Table 1. Fig. 3 shows the results of the COMSALT simulations for two of the model parameters for different values of the shear velocity u_*: the average number of reptating particles per saltator impact n (Fig. 3a), and the average number of saltator impacts on a flat bed N_{im}^0 (Fig. 3b). The third model input for the ripple model simulated by COMSALT is the probability distribution of the reptation length, which is shown at different shear velocities in Fig. 4. We find that the probability distribution of reptation length of 100 μm particles on Mars is given by

$$p(\alpha) = [1 - \exp(-\sqrt{x/s})](a/x)\exp(-\sqrt{x/b}), \tag{7}$$

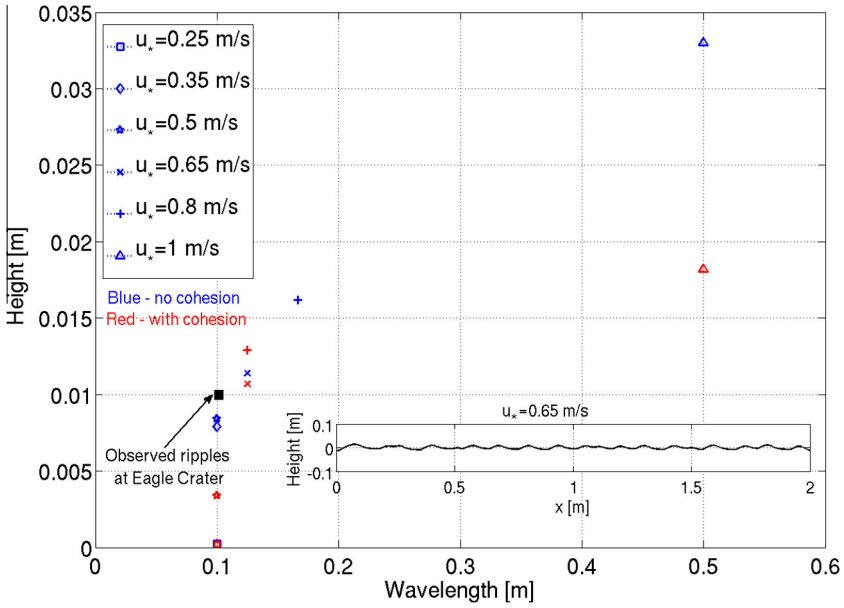

Fig. 5. Model simulations (Eq. (5)) of ripples on Mars with parameters computed by COMSALT (see Figs. 3 and 4) for different shear velocities after 25 Earth hours. The inset shows the final ripples profile for $u_* = 0.65$ m/s.

where the numerical constants are $s = 0.00039$ m, $a = 0.215$, and $b = 0.0277$ m (also see Fig. 4). To the best of our knowledge, this is the first numerically obtained probability distribution of reptation length and it differs from the distributions used previously in mathematical models of sand ripples. For instance, Anderson (1987a,b) and Yizhaq et al. (2004) used an exponential distribution, whereas Manukyan and Prigozhin (2009) used a normal distribution. It is important to note that $p(\alpha)$ is independent of u_*, which is in agreement with experimental and theoretical studies of sand transport that state that the mean reptation length scales with the grain diameter (Andreotti et al., 2006).

Fig. 5 shows the wavelength and height of the simulated ripples for different shear velocities after 25 Earth hours. Based on these simulations it can be concluded that the observed basaltic ripples at Eagle Crater (1 cm height and wavelength of 10 cm) could be formed under the action of winds with shear velocities $0.35 < u_* < 1$ m/s, which is much below the estimated fluid threshold on Mars for the 100 μm grain size of $u_{*th} \approx 1.5$ m/s.

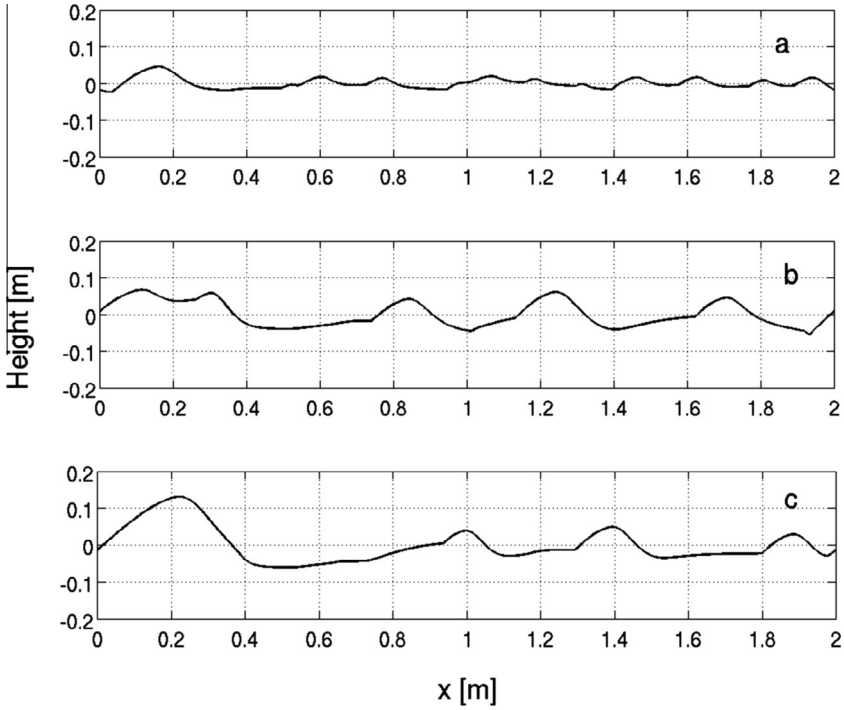

Fig. 6. (a) Modeled ripples profiles for $u_* = 1.6$ m/s (with cohesion) after 8 h, 16 h (b) and 25 h (c). For this high wind velocity the ripples become quite large with 1 m wavelength. On Earth, normal ripples are much smaller and their wavelength generally does not exceed 30 cm (Bagnold, 1941).

For $u_* > 1$ m/s the ripples grow very fast and reach large dimensions, as shown in Fig. 6 for $u_* = 1.6$ m/s. On Earth, such ripples are considered as megaripples and a bimodal distribution of grain size is needed for their formation (Yizhaq et al., 2012a,b). We find that normal ripples on Mars can grow much larger than their terrestrial analogs. The large ripples (wavelength ~2 m) that were observed at El Dorado were classified as normal ripples (Sullivan et al., 2008) because their crest particles (300 μm) moved in saltation and not in reptation or creep. The mechanism that leads to such large normal ripples is still unknown as the physical process which leads to saturation of ripple growth is not fully understood (Andreotti et al., 2006).

The evolution of the mean ripple height and wavelength are shown in Fig. 7a and b, respectively. The abrupt increase in the wavelength is due to the decrease in the number of crests because of the coalescence of smaller ripples (Fig. 7c). This coarsening process causes the number of crests to decrease sharply during the first 5 h, after which it changes much slower. Thus, after 1 day of simulations, the ripple growth is quite slow.

For low shear velocities like $u_* = 0.15$ m/s and $u_* = 0.25$ m/s the ripple height and wavelength remains very small even after one full martian day of sand transport driven by unidirectional wind. Thus, the basaltic ripples at Eagle Crater were probably not formed under the action of these weak winds because the process is very slow and would require an extended period of unidirectional wind. According to Sullivan et al. (2005), the recent wind events at Eagle Crater included cycles of winds coming from 315° or 135°, such that the wind is most likely not unidirectional for long periods of time.

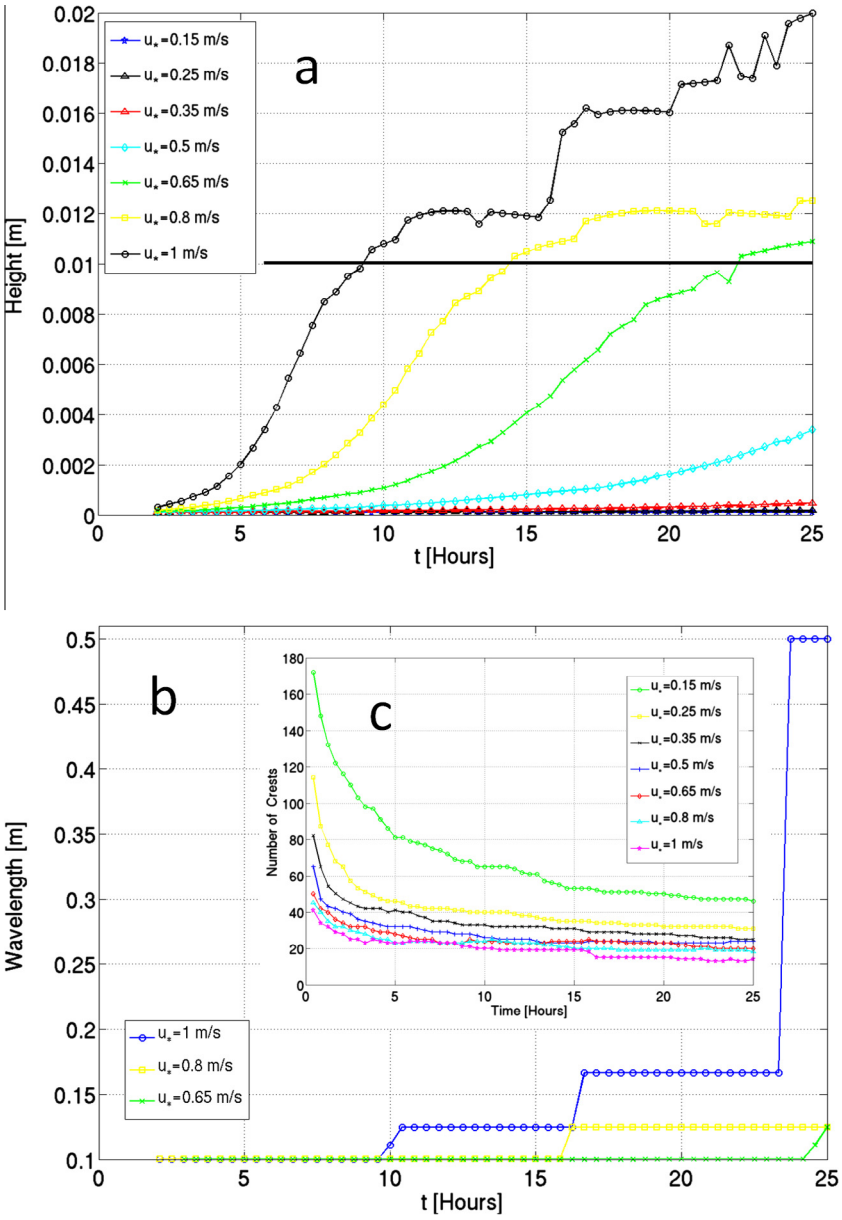

Fig. 7. (a) Time evolution of ripple height for different shear velocities. For $u_* < 0.35$ m/s, the ripples remain very small, whereas for $u_* = 0.8$ m/s their average height reaches 1 cm after 10 h. The thick black line indicates the observed height of the basaltic ripples (1 cm) (Sullivan et al., 2005). (b) Time evolution of ripple wavelength for three shear velocities. The increase in the wavelength is due to ripples merging. (c) Time evolution of the number of ripple crests in the simulation domain (2 m); the number of crests decreases in time due to ripples merging. At long simulation times (~25 h), the number of crests decreases much more slowly than at the start of the simulation. The inset shows the ripple profiles for $u_* = 0.5$ m/s at different times. After 16 h of simulations the ripples have the same dimensions of the basaltic ripples at Eagle crate.

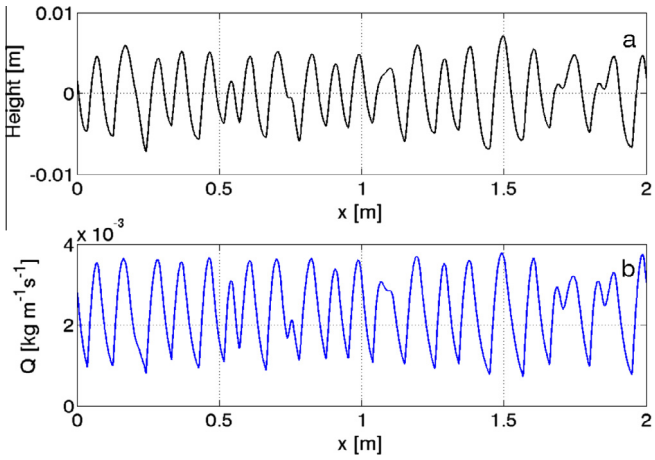

Fig. 8. (a) Ripple profile after 16 h for $u_* = 0.5$ m/s. (b) The reptation flux (Q) along the profile. Note that the flux is maximal at the ripple crests and minimal at the troughs. The average reptation flux is 9.35×10^{-5} kg m^{-1} s^{-1}.

The observed ripple height of 1 cm and wavelength of 10 cm is reached at different times for ripples developed under different shear velocities. For example, for $u_* = 0.65$ m/s it takes 15 h, for $u_* = 0.8$ m/s it takes 10 h, and for $u_* = 0.5$ and $u_* = 0.35$ it will take more than one martian sol to reach the observed ripple dimensions (see Fig. 7). Thus, based on these simulations, we cannot define the shear velocity that formed the ripples at Eagle Crater exactly. However, our simulations are consistent with the idea that hysteresis allows the formation of these 100 μm ripples (Kok, 2010a).

Fig. 8 shows the calculated reptation flux, defined by Eq. (2), along the profile of ripples that developed under $u_* = 0.5$ m/s wind. As expected, the flux is maximal near the ripple crest and its minimum value occurs at the trough. The mean value of the reptation flux is 9.35×10^{-5} kg m^{-1} s^{-1}. The assumption that this wind blows during the whole year gives 2952 kg m^{-1} yr^{-1}. The reptation flux can be calculated by using the bulk density of the sand, 1950 kg m^{-3} [equal to $(1 - \lambda_p)\rho$] which yields a reptation flux of 1.51 m^3 m^{-1} yr^{-1}. The mean reptation flux was estimated from ripple migration measurements at the Nili Patera dune field as 1.4 ± 0.08 m^3 m^{-1} yr^{-1} (Bridges et al., 2012b). Our value likely overestimates the long-term reptation flux, as we assumed that the wind blows in one direction with this speed over the entire year, which is unrealistic. As we do not know the wind speed distribution at Eagle Crater, we use our estimation as an upper limit for the reptation flux.

Fig. 9 shows the average reptation flux in m^3 m^{-1} yr^{-1} for different shear velocities as calculated from the ripple simulations. Based on the COMSALT results (Fig. 3b), we can calculate the saltation flux for 100 μm spherical basaltic grains with a density of 3000 kg m^{-3}. The inset of Fig. 9 shows the ratio between the saltation flux to the reptation flux at ripple crest as a function of the shear velocity. This ratio is large for small shear velocities and becomes smaller (~10) for high wind speeds as the ejection of reptating particles becomes more efficient. Bridges et al. (2012b) found that this ratio was equal to approximately four at the Nili Patera dune field. One possible explanation for the difference between our results and the result at Nili Patera is that Bridges calculated the reptation flux from ripple migration. These ripples were quite large with a mean wavelength of 4.6 m and their mean height was estimated to be 45 cm by assuming a ripple index of 10 (the ratio between wavelength to height). The particle size of Nili Patera ripples is not known and it might be different than 100 μm. Larger grains would imply a more efficient splash process due to the decreasing effect of cohesion, which would reduce the ratio of the reptation to the saltation flux. Another likely explanation is that the winds at Nili Patera may be stronger than the wind we used in our simulations, as this ratio tends to be smaller for higher wind speeds.

4. Conclusions

Here we for the first time combine a detailed numerical saltation model (COMSALT) with a model for ripple formation. We used

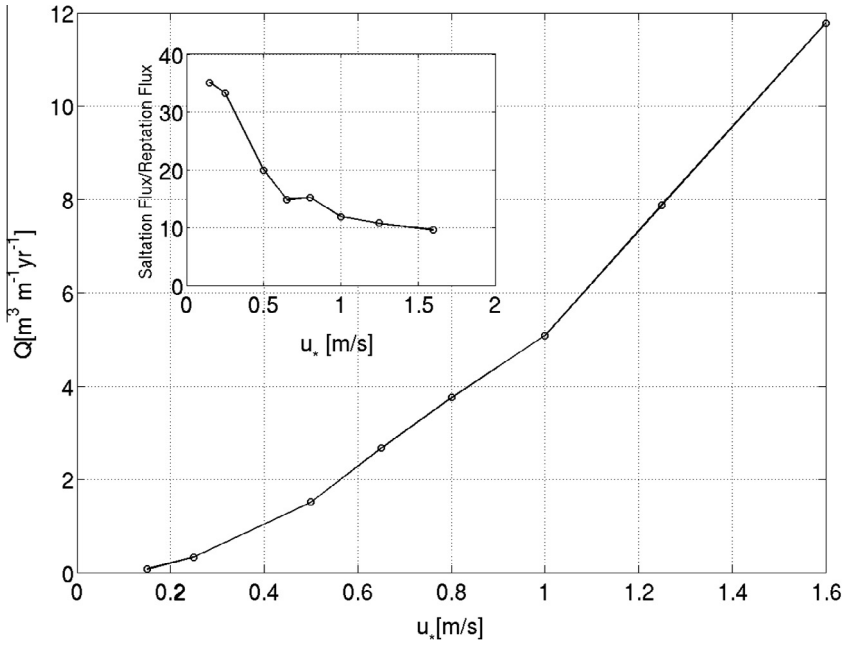

Fig. 9. Mean annual reptation flux calculated from ripple simulations (after 25 h) for different shear velocities. We assume a year-round constant wind speed, which is unrealistic. The inset shows the ratio of the reptation and saltation fluxes (calculated using COMSALT results) for 100 μm particles. The ratio becomes smaller for higher winds speed (see text for discussion).

these coupled models to simulate the formation of the 100 μm basaltic ripples at Eagle Crater on Mars, whose formation is poorly understood (Sullivan et al., 2005). Our results indicate that these small ripples can be developed by shear velocities of ~0.35 m/s or greater, and thus much below the fluid threshold estimated at ~1.5 m/s for 100 μm particles on Mars (Iversen and White, 1982). In light of these and previous findings (Sullivan et al., 2005; Kok, 2010a), we envision that most sand transport on Mars occurs as follows. Individual high-speed eddies lift surface particles and momentarily suspend them. However, the large terminal fall speed of these particles will cause them to exit the high-speed eddy within seconds. Upon impacting the surface, these particles initiate saltation, which can then be sustained downwind by wind speeds by relatively weak winds that can be approximately up to an order of magnitude less than that of the high-speed turbulent eddy that lifted the particles (Kok, 2010a, b).

In addition, the reptation flux for these ripples is similar to the recently estimated reptation flux at the Nili Patera dune field (Bridges et al., 2012b). These findings can be regarded as indirect evidence for the occurrence of substantial hysteresis in martian saltation, and support the observed migration of dunes and ripples despite the limited occurrence of winds capable of initiating sand transport in the low-density atmosphere of Mars.

Acknowledgments

We thank Robert Sullivan for providing us the picture used in Fig. 1 and its description. We thank Daniela Tirsch and Claire Newman for their constructive reviews, which improved the quality of the manuscript. This work was supported by the German-Israeli Foundation for Scientific Research and Development (GIF Research Grant No. 1143-60.8/2011).

References

Almeida, M.P., Parteli, E.J.R., Andrade, J.S., Herrmann, H.J., 2008. Giant saltation on mars. Proc. Natl. Acad. Sci. USA 105, 6222–6226.
Anderson, R.S., 1987a. Eolian sediment transport as a stochastic process—The effects of a fluctuating wind on particle trajectories. J. Geol. 95, 497–512.
Anderson, R.S., 1987b. A theoretical model for aeolian impact ripples. Sedimentology 34, 943–945.
Anderson, R.S., 1990. Eolian ripples as examples of self-organization in geomorphological systems. Earth-Sci. Rev. 29, 77–96.
Andreotti, B., Claudin, P., Pouliquen, O., 2006. Aeolian sand ripples: Experimental study of fully developed states. Phys. Rev. Lett. 96. Article number: 028001.
Bagnold, R.A., 1941. The Physics of Blown Sand and Desert Dunes. Methuen, London.
Basu, S., Richardson, M.I., Wilson, R.J., 2004. Simulation of the martian dust cycle with GFDL Mars GCM. J. Geophys. Res. 109, E11006. http://dx.doi.org/10.1029/2004JE002243.
Beladjine, D., Ammi, M., Oger, L., Valance, A., 2007. Collision process between an incident bead and a three-dimensional granular packing. Phys. Rev. E 75. Article number: 061305.
Bourke, M.C., Edgett, K.S., Cantor, B.A., 2008. Recent aeolian dune change on Mars. Geomorphology 94, 247–255.
Bourke, M.C., Lancaster, N., Fenton, L.K., Parteli, E.J.R., Zimbelman, J.R., Radebaugh, J., 2010. Extraterrestrial dunes: An introduction to the special issue on planetary dune systems. Geomorphology 121, 1–14.
Bridges, N.T. et al., 2012a. Planet-wide sand motion on Mars. Geology 40 (1), 31–44.
Bridges, N.T., Ayoub, F., Leprince, S., Lucas, A., Mattson, S., 2012b. Earth-like sand fluxes on Mars. Nature. http://dx.doi.org/10.1038/nature11022.
Chojnacki, M., Burrm, D.M., Moersch, J.F., Michaeles, T.I., 2011. Orbital observations of contemporary dune activity in Endeavor Crater, Meridiani Planum, Mars. J. Geophys. Res. 116, E00F19. http://dx.doi.org/10.1029/2010JE003675.
Claudin, P., Andreotti, B., 2006. A scaling law for aeolian dunes on Mars, Venus, Earth, and for subaqueous ripples. Earth Planet. Sci. Lett. 252 (1–2), 30–44.
Edgett, K.S., 2002. Low-albedo surfaces and eolian sediment: Mars Orbiter Camera views of western Arabia Terra craters and wind streaks. J. Geophys. Res. (Planets) 107, 5038–5068.
Edgett, K.S., Christensen, P.R., 1991. The particle size of martian aeolian dunes. J. Geophys. Res. 96 (E5), 22762–22776.
Edgett, K.S., Christensen, P.R., 1994. Mars aeolian sand: Regional variations among dark-hued crater floor features. J Geophys Res. 99 (E1), 1997–2018.
Fausett, L.V., 1999. Applied Numerical Analysis Using Matlab. Prentice Hall, Upper Saddle River, NJ 07458.
Fenton, L.K., Michaels, T.I., 2010. Characterizing the sensitivity of daytime turbulent activity on Mars with the MRAMS LES: Early results. Mars 5, 159–171.
Greeley, R., Iversen, J.D., 1985. Wind as a Geological Process on Earth, Mars, Venus, and Titan. Cambridge Univ. Press, New York.
Haberle, R.M., Houben, H.C., Hertenstein, R., Herdtle, T., 1993. A boundary-layer model for Mars: Comparison with Viking lander and entry data. J. Atmos. Sci. 50, 1544–1559.
Holstein-Rathlou, C. et al., 2010. Winds at the Phoenix landing site. J. Geophys. Res. 115, E00E18.
Iversen, J.D., White, B.R., 1982. Saltation thresholds on Earth, Mars, and Venus. Sedimentology 29, 111–119.
Jerolmack, D.J., Mohrig, D., Grotzinger, J.P., Fike, D.A., Watters, W.A., 2006. Spatial grain size sorting in eolian ripples and estimation of wind conditions on planetary surfaces: Application to Meridiani Planum, Mars. J. Geophys. Res. 111, E12S02. http://dx.doi.org/10.1029/2005JE002544.
Kok, J.F., 2010a. Differences in the wind speeds required for initiation versus continuation of sand transport on Mars: Implications for dunes and sand storms. Phys. Rev. Lett. 104. Article number: 074502.
Kok, J.F., 2010b. An improved parameterization of wind-blown sand flux on Mars that includes the effect of hysteresis. Geophys. Rev. Lett. 37. Article number: L12202.
Kok, J.F., 2012. Martian sand blowing in the wind. Nature 485, 312–313. http://dx.doi.org/10.1038/nature11193.
Kok, J.F., Renno, N.O., 2009. A comprehensive numerical model of steady state saltation (COMSALT). J. Geophys. Res. 114, D17204. http://dx.doi.org/10.1029/2009 JDO11702.
Kok, J.F., Parteli, E.J.R., Michaels, T., Bou Karam, D., 2012. The physics of wind-blown sand and dust. Rep. Prog. Phys. 75. Article number: 106901.
Manukyan, E., Prigozhin, L., 2009. Formation of aeolian ripples and sand sorting. Phys. Rev. E 79, 031303. http://dx.doi.org/10.1103/PhysRevE.79.031303.
Merrison, J.P. et al., 2007. Determination of the wind induced detachment threshold for granular material on Mars using wind tunnel simulations. Icarus 191, 568–580.
Nemoto, M., Nishimura, K., 2004. Numerical simulation of snow saltation and suspension in a turbulent boundary layer. J. Geophys. Res. 109, D18206. http://dx.doi.org/10.1029/2004JD004657.
Parteli, E.J.R., Herrmann, H.J., 2007. Dune formation on the present mars. Phys. Rev. E 76, 041307.
Pähtz, T., Kok, J.F., Herrmann, H.J., 2012. The apparent roughness of a sand surface blown by wind from an analytical model of saltation. N. J. Phys. 14, 043035, 43pp.
Rioual, F., Valance, A., Bideau, D., 2003. Collision process of a bead on a two-dimensional bead packing: Importance of the inter-granular contacts. Europhys. Lett. 61, 194–200.
Schofield, J.T., Barnes, J.R., Crisp, D., Haberle, R.M., Larsen, S., et al., 1997. The Mars Pathfinder atmospheric structure investigation meteorology (ASI/MET) experiment. Science 278, 1752–1758.
Shao, Y.P., McTainsh, G.H., Leys, J.F., Raupach, M.R., 1993. Efficiencies of sediment samplers for wind erosion measurements. Aust. J. Soil Res. 31, 519–532.
Sharp, R.P., 1963. Wind ripples. J. Geol. 71, 617–636.
Silvestro, S., Fenton, L.K., Vaz, D.A., Bridges, N.T., Ori, G.G., 2010. Ripple migration and dune activity on Mars: Evidence for dynamic wind processes. Geophys. Rev. Lett. 37, L20203. http://dx.doi.org/10.1029/2010GL044743.
Squyres, S.W. et al., 2006. Overview of the Opportunity Mars Exploration Rover mission to Meridiani Planum: Eagle Crater to purgatory ripple. J. Geophys. Res. 111, E12S12. http://dx.doi.org/10.1029/2006JE002771.
Sullivan, R., Banfield, D., 2005. Transition between aeolian saltation and suspension on Earth and Mars. Eos Trans. American Geophysical Union 86(52) (Fall Suppl.). Abstract H31G-02.
Sullivan, R. et al., 2005. Aeolian processes at the Mars Exploration Rover Meridiani Planum landing site. Nature 436. http://dx.doi.org/10.1038/nature03641.
Sullivan, R. et al., 2008. Wind-driven particle mobility on mars: Insights from Mars Exploration Rover observations at "El Dorado" and surroundings at Gusev Crater. J. Geophys. Res. 113, E06S07.
Wilson, J.D., Sawford, B.L., 1996. Review of Lagrangian stochastic models for trajectories in the turbulent atmosphere. Bound. Layer Meteorol. 78, 191–210.
Yizhaq, H., Balmforth, N.J., Provenzale, A., 2004. Blown by wind: Nonlinear dynamics of aeolian sand ripples. Physica D 195, 207–228.
Yizhaq, H., Katra, I., Isenberg, O., Tsoar, H., 2012a. Evolution of megaripples from a flat bed. Aeolian Res. 6, 1–12.
Yizhaq, H., Katra, I., Kok, J.F., Isenberg, O., 2012b. Transverse instability of megaripples. Geology 40, 459–462.
Zimbelman, J.R., 2000. Non-active dunes in the Acheron Fossae region of between the Viking and Mars Global Surveyor eras. Geophys. Res. Lett. 27 (7), 1069–1072.
Zimbelman, J.R., Irwin III, R.P., Williams, S.H., Bunch, F., Valdez, A., Stevens, S., 2009. The rate of granule ripple movement on Earth and Mars. Icarus 203, 71–76.